

# Origins of anomalous Raman exponents in single molecule magnets

Lei Gu and Ruqian Wu\*

*Department of Physics and Astronomy, University of California, Irvine, CA 92697-4575, USA.*

E-mail: wur@uci.edu

## Abstract

The Raman exponent of single molecular magnetic relaxation may take various unexpected values because of rich phonon spectrum and spin-phonon coupling of molecular crystals. We systematically examine the origins of different abnormalities, and clarify misunderstandings in the past, particularly the appropriateness of the fitting procedures for the exponents. The dominance of the Raman process has been shown to occur along with the emergence of magnetic hysteresis, and this regime is probably most suitable for practical applications of single molecule magnets. After reshaping our understanding of the Raman process in spin relaxation, we propose guiding rules for slowing it down.

The spin-vibration and spin-phonon couplings in solids and molecules are widely discussed in textbooks but are puzzling in many cases such as magnetic phase transition, damping and relaxation. These issues are even more significant and complex in dealing with single molecule magnets (SMMs) which have received increasing attention as possible qubits for quantum information processing and storage.<sup>1,2</sup> In fact, the control of spin-vibration coupling in SMMs by selecting appropriate ligands and substrates is the most viable strategy to lower

their relaxation rate or equivalently to extend their quantum coherence time. Obviously, it is necessary and urgent to clarify the effect of vibrational excitations on spin relaxation of SMMs such as via the Raman process, so that comprehensive understanding in their quantum behaviors and practical design rules for SMM-based devices can be established.

In the past three decades, considerable advancements have been made for the synthesis and characterization of complex molecules and molecular solids.<sup>3-16</sup> The judiciously designed dysprosoceniums<sup>15-18</sup> show magnetic hysteresis at the liquid nitrogen temperature, indicating the possibility for the use in SMM-based devices. Single magnetic molecules were used to functionalize tips of scanning tunneling microscopy (STM) for measuring and mapping exchange interactions with a sub-Angstrom spatial resolution.<sup>19,20</sup> Strong intermixing between vibrational and spin excitation were also directly detected in the inelastic electron tunneling spectrum (IETS),<sup>21</sup> which provides a useful tool to quantitatively investigate and engineer molecular magnetic systems. However, theoretical developments in this realm have not kept the pace with the experimental counterpart, leaving many long-standing puzzles that call for fundamental studies. One of the outstanding issues is the presence of anomalous Raman exponents (see e.g.<sup>5,11,16,22-27</sup>) that generally deviates from the standard values.<sup>28,29</sup> Considering that the magnetic hysteresis usually occurs jointly with the dominance of Raman relaxation,<sup>15,16</sup> the Raman regime appears to be suitable for computing and sensing applications and deserves careful investigations.

Most SMMs designed for slow magnetic relaxation have strong uniaxial magnetic anisotropy (see Ref. 9 for an exception), described by  $H_S = -DS_z^2 - E(S_x^2 - S_y^2)$  with  $D \gg E$ . This sets an effective barrier  $U_{eff} = DS^2$  for the standard Orbach relaxation pathway as sketched in Fig. 1a. In Ref. 30, we clarified that the Raman processes for the transitions in this pathway cannot lead to power laws,<sup>15</sup> as the Orbach barrier set the time scale  $\tau = \tau_0 e^{U_{eff}}$  and the Raman processes somewhat modify the prefactor  $\tau_0$ . This implies that the power laws can only arise from the direct tunneling between the ground state doublet. The significant Raman process conventionally referred to should be the one shown in Fig. 1b, that is, direct

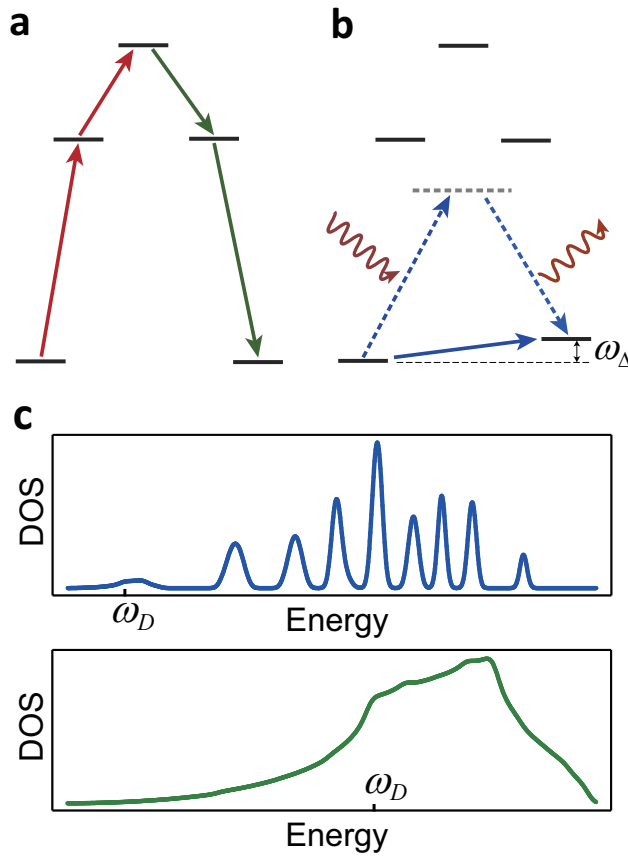


Figure 1: **a**, When the relaxation process is mediated by excitation states, Raman processes of these transitions do not yield power law dependencies, which can only result from direct tunneling between the ground state doublet as shown in **b**. **c**, Phonons of a SMMs system (upper) are made of acoustic phonons with very low energy and optical phonons from broadening of local vibrational modes; this difference with bulk materials (lower) brings about several peculiarities to the Raman processes in SMMs, and gives rise to the abnormalities.

tunneling mediated by simultaneously absorbing and emitting of a phonon.

At high temperature, all spin states are well accessible, so the Orbach process dominates the magnetic relaxation. When the temperature is reduced, the Raman process can be dominant and power laws emerge. The intriguing cooccurrence of magnetic hysteresis and emergence of the power law can be understood by the change of the  $\tau - T$  dependence itself. In the Orbach regime, a small temperature reduction can dramatically increase the relaxation time, especially for large Orbach barriers. When reaching the Raman regime, this sensitivity is significantly weakened because of the transition to a power law  $\tau - T$  relation (cf. Eq. (1)). When experimentalists try to make a tradeoff between high temperature and long relaxation time, this transition point is likely to be “selected” as the emergence point of magnetic hysteresis. Since only the ground state doublet is involved in the spin dynamics, another merit of the Raman regime for practical applications is the purity, i.e., the system is a desired two state qubit.

With relaxation times ( $\tau$ ) of a SMM in a wide temperature range, typical  $\tau - T$  curves can be fitted by a relation

$$\tau = \tau_0 e^{\frac{U_{eff}}{k_B T}} + CT^{-n}. \quad (1)$$

The first term represents the Orbach process, and the second term is mainly due to the Raman process. The standard Raman exponent at low temperature should be  $n = 7, 8, 9$ .<sup>28,29</sup> Nevertheless, exponents this big has been rarely observed in SMMs, and a large bulk of observations gives  $n = 3 \sim 5$  (see e.g.<sup>5,11,16,22-27</sup>). These unconventional values are usually left unexplained or ascribed to the optical-acoustic mechanism.<sup>31</sup> However, most of SMMs with slow magnetic relaxation was designed to have strong uniaxial magnetic anisotropy ( $D \ll E$ ), so that their Orbach barriers are high. This makes the splitting between the ground state doublet small and implies that the absorbed and emitted phonons in the Raman process should be of the same type. As a result, the optical-acoustic mechanism is inapplicable, and other mechanisms should be explored for the explanation of anomalous Raman exponents for the spin relaxation in SMMs.

We found that the profile of phonon density of states (DOS) of SMM systems may lie at the heart of these abnormalities. Since the magnetic measurements are usually performed on molecule crystals consisting of the magnetic complexes and solvent molecules, we used a 3D oscillator model to show generic traits of the phonon DOS. Using a  $3 \times 3 \times 3$  supercell, and assuming that the intra-cell ionic force constant is one order bigger than the inter-cell van der waals type ones, the phonon DOS of typical molecular crystals is generated as given in the upper panel of Fig. 1c. The comparison between the phonon DOS curves of ordinary crystals (lower panel) clearly demonstrates the reason why the conventional Raman exponents cannot arise in SMMs. The derivation relies on extending the integration limit  $\omega_D/T$  of the Debye integral (cf. Eq. (2)) to the infinity. However, because  $\omega_D$  is small in typical SMMs systems, such extension becomes inapplicable to SMMs. In the following, we will investigate, from three aspects, how the small Debye energy and the discrete nature of optical phonons affect the Raman exponent.

From the second order spin-phonon coupling Hamiltonian, the tunneling rate can be derived as

$$p = N(\omega_\Delta) \iint \frac{\pi |a_{qq'}|^2}{2\omega_q \omega_{q'}} d\omega_q d\omega_{q'} \rho(\omega_q) \rho(\omega_{q'}) \{ [N(\omega_q) + N(\omega_{q'}) + 1] \delta(\omega - \omega_q - \omega_{q'}) + [N(\omega_q) - N(\omega_{q'})] \delta(\omega + \omega_q - \omega_{q'}) \}, \quad (2)$$

where  $\omega_q$  denotes phonon frequency,  $N(\omega_q)$  the Bose-Einstein distribution,  $\rho(\omega_q)$  the phonon DOS, and  $\omega_\Delta$  the energy difference between the ground state doublet as shown in Fig. 1b. By energy conservation, we may identify the first term as the double phonon process whereby two phonons are absorbed, and the second terms as the Raman process whereby a phonon is absorbed ( $\omega_{q'}$ ) and a phonon of lower energy is emitted ( $\omega_q$ ). Here, we include the double phonon process since it is naturally derived from the Hamiltonian of second order spin-phonon coupling. In other words, the Raman process is inevitably accompanied by the double phonon process. In most experiments, alternating current (a.c.) magnetic relaxation

is measured, and the a.c. magnetic field breaks the time-reversal symmetry. We focus on the case of non-Kramers doublets. One may refer to Refs. 9,29 for the derivation and discussion on the magnetic relaxation of Kramers doublets.

In the long wavelength limit, the continuum mechanics applies,<sup>28,32</sup> which implies that the lattice deformation caused by acoustic phonons is approximately proportional to the phonon momentum. As phonon-spin coupling essentially reflects variation of electronic state due to the lattice deformation, this proportionality applies to the coupling strength, i.e.,  $|a_{qq'}| \propto |q||q'|$ . According to the Debye dispersion  $\omega_q \propto |q|$ , the coupling coefficient can be approximated as  $|a_{qq'}| \propto \omega_q \omega_{q'}$ . Together with Debye phonon DOS  $\rho \propto \omega^2$ , the second term of Eq. (2) gives the Debye integrals for the Raman process. The standard Raman exponents arise when the integration limit  $\omega_D/k_B T$  is extended to the infinite. As a result, we obtain  $p \propto T^6 N(\omega_\Delta)$ . High temperature or small  $\omega_\Delta$  expansion of  $N(\omega_\Delta)$  results in  $\tau^{-1} \propto p \propto T^7/\omega_\Delta$ , the standard relation for the non-Kramers doublets.

The requirement  $\omega_D \gg k_B T$  for legitimacy of the integration limit extension, however, is generally not satisfied in SMMs. A small Debye energy relative to the temperature is the first aspect that gives rise to anomalous Raman exponents. Because of the weak inter-molecular interaction, the acoustic phonons mainly represent the inter-molecule motion.<sup>30</sup> Assuming that the inter-molecular interaction is one order weaker than the intra-molecular interactions and masses of the molecules are one order larger than an ordinary atom, the Debye energies of SMMs are one order smaller than those of ordinary crystals, and  $\omega_D \lesssim 10 \text{ cm}^{-1}$  is a reasonable estimation. As  $\omega_D = 10 \text{ cm}^{-1}$  amounts to 14.4 K, the conventional Raman exponent is appropriate only when the temperature is as low as  $T \sim 1 \text{ K}$ .

On the contrary, in SMMs the condition  $\omega_D \ll k_B T$  can be well satisfied, which implies that the Debye phonons are well accessible (Fig. 2b). With high temperature expansion of the Bose-Einstein function  $N(\omega_q)$ , the second term of Eq. (2) gives  $\tau^{-1} \propto T^2$ . This value agrees with the observation 2.15 in Ref. 15. Phonon DOS not in perfect Debye form and variation of spin-phonon coupling strength with momentum may cause small deviations. In this regard,

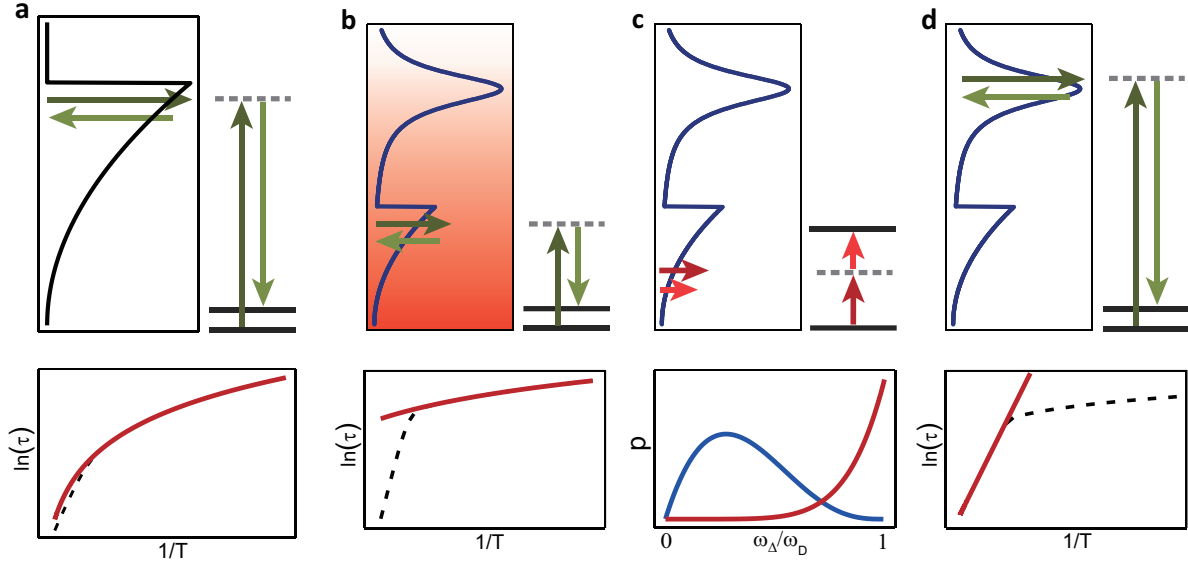


Figure 2: **a**, The conventional Raman process is mediated by acoustic phonons in solids having a large Debye energy. **b**, Because of a small Debye energy, the acoustic phonons in SMM systems are well accessible for relatively high temperature, leading to  $\tau^{-1} \propto T^2$ . **c**, For SMMs with large angular momentum, the Zeeman splitting can be comparable with the Debye energy, and the double phonon process (red) can perceptibly contribute to the tunneling rate, even surpassing the Raman process (blue). **d**, Raman process due to a local vibration yields an exponential dependence, which is a major cause of anomalous Raman exponents.

this observation is not an abnormality but a clear case of high temperature Raman process.<sup>33</sup> In bulk materials, due to large Debye energies, the high temperature expansion is rarely used. But in SMMs, the high temperature Raman process can be essential and constitutes an origin of small Raman exponents.

In the double phonon process, transition among spin states are accompanied by emission or absorption of two phonons. Because of the energy conservation  $\omega_q + \omega_{q'} = \omega_\Delta$ , only phonons in the range  $[0, \omega_\Delta]$  can contribute to the direct tunneling. In contrast, phonons in the range  $[0, \omega_D]$  participate in the Raman relaxation process. For small splitting and large Debye energy ( $\omega_\Delta \ll \omega_D$ ), the double phonon process is inconsiderable compared to the Raman process and has rarely been mentioned. As  $\omega_D$  is small in SMMs and the Zeeman splitting may be sizable for large spins, the relative contribution of these two processes are worth of careful investigation.

Our numerical estimation shows that for  $\omega_D = 10 \text{ cm}^{-1}$ , the double phonon process surpass the Raman process when  $\omega_\Delta/\omega_D \gtrsim 0.7$  (Fig. 2c). At very low temperature ( $T < 3 \text{ K}$ ), only the low energy phonons are effective for both processes and the phonons in the range  $[\omega_\Delta, \omega_D]$  are less important, so the critical ratio can be largely reduced (see supplementary). In general, because of the small splitting between the ground state doublet, the double phonon process can be safely neglected for SMMs with strong uniaxial magnetic anisotropies. For example, a 1000 Oe magnetic field yields an  $1.4 \text{ cm}^{-1}$  Zeeman splitting between  $|\pm S\rangle$  for  $S = 15/2$ . As  $\omega_\Delta/\omega_D \ll 1$ , this does not lead to strong double phonon processes. Therefore, the double phonon process is still an insignificant relaxation channel, except for extremely strong magnetic field and low temperature, which results in large  $\omega_\Delta$  or small critical  $\omega_\Delta/\omega_D$  ratio, respectively.

Most recently, the mechanism of under-barrier relaxation in absorbate magnetic atoms<sup>34</sup> and SMMs<sup>5,6,11,24,25,35-43</sup> has been explained.<sup>30,34</sup> It is found that the Raman process due to a vibrational mode can yield exponential temperature dependence  $\tau = \tau_0 e^{U_{vib}/k_B T}$  as shown in Fig. 2d. This means that the vibrational mode raises an effective relaxation barrier equal

to its energy. The exponential form implies that the conventional use of Eq.(1) for fitting is a long standing misstep, since the actual temperature dependence is an exponential function or summation of a series of them. When forcefully fitting it with a power law  $\tau \propto T^{-n}$ , exponents unrelated to the conventional Raman process might be obtained. This vibronic barrier is the third aspect concerning the anomalous Raman exponents, supposedly the most significant one.

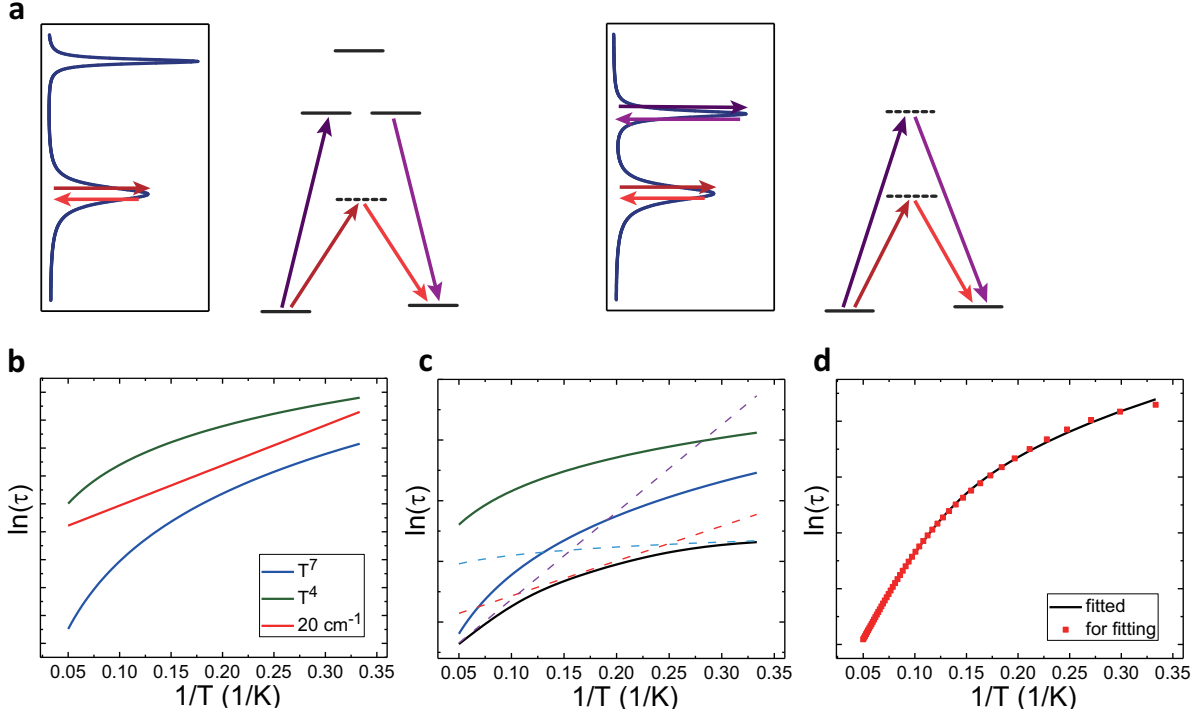


Figure 3: **a**, Two cases where small Raman exponents could be deduced from Eq.(1). **b**, Exponential dependence of an energy barrier  $20 \text{ cm}^{-1}$  is similar with  $\tau^{-1} \propto T^4$ , and more clearly different with  $\tau^{-1} \propto T^7$ . **c**, When summed up with exponential dependence of a higher energy barrier and  $\tau^{-1} \propto T$  for the direct process, the curve (black) can be quite deceptive and easily mistaken as  $\tau \propto T^4$ . **d**, In this example, such a summed curve can be well fitted by Eq. (1) with exponent  $n = 4.02$ .

We take a vibrational mode  $\omega = 20 \text{ cm}^{-1}$  for instance. As shown in Fig. 3b, the curve of  $\tau^{-1} \propto e^{20/K_B T}$  has similar variation range with  $\tau^{-1} \propto T^4$  than with  $\tau^{-1} \propto T^7$ , the standard value for non-Kramers doublet. Note that the Raman process mediated by this mode is not the only relaxation channel. At high temperature, the relaxation is dominated by the Orbach process (left Fig. 3a) or another intra-molecular vibrational mode (right Fig. 3a) with

stronger coupling with the spin than this mode. This adds another exponential function as denoted by the dotted purple line in Fig. 3c (here a  $50 \text{ cm}^{-1}$  barrier is assumed). In the other side, the direct process can be dominant at low temperature and raises power law  $\tau \propto T^{-1}$ .<sup>28,29</sup> When these two additional functions are included, we have the black curve in Fig. 3c, which is a generic curve from most experimental measurements. Compared with  $\tau \propto T^{-4}$ , it is quite deceptive and can be easily mistaken (here the position is not important due to the  $\ln(\tau)$  form). In Fig. 3d, we fit the curve with Eq. (1), which leads to an exponent  $n = 4.02$ . Typically, there are many vibrational modes of SMMs in the range  $10 \sim 30 \text{ cm}^{-1}$ . The variations of the mode energies and relative contributions from the three relaxation processes are expected to cause derivations from  $n = 4$ . Therefore, the improper fitting with Eq. (1) may give diverse exponents in the range  $3 \sim 5$ .

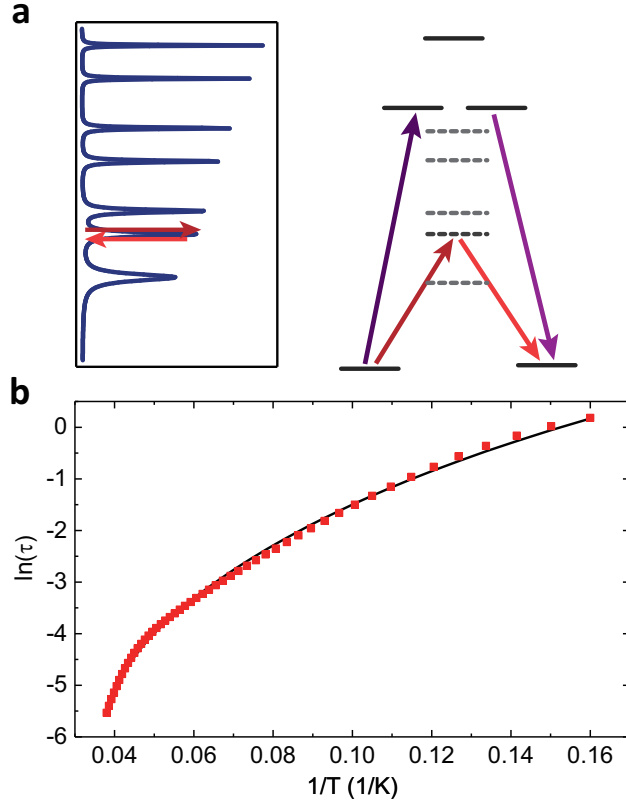


Figure 4: **a**, When the Orbach barrier is high, the vibrational modes below it collectively contribute to the Raman relaxation **b**, Summation of a series of exponential functions still leads to deceptive curves that may be mistaken as a power function. Using Eq. (1), the data (red) can be fitted with an exponent  $n = 3.55$ .

The above case applies when the zero field splitting is small and only a few vibrational modes have lower energies. When the zero splitting is large, many vibrational modes having energies lower than the Orbach barrier may collectively contribute to the Raman relaxation (Fig. 4a). To validate our approach, we calculated the vibrational modes of the Co-NCCN metallacycles with the ORCA package.<sup>44</sup> According to Ref. 41, it is a spin-3/2 molecule with uniaxial anisotropy  $D = 115 \text{ cm}^{-1}$ , i.e., an Orbach barrier of  $230 \text{ cm}^{-1}$ . Summing up the exponential function for 24 modes below the Orbach barrier, we obtained the curve in Fig. 4b, which is close to the experimental result. Fitting the curve with Eq. (1) gives a Raman exponent of  $n = 3.55$ . The first order and second order spin-phonon coupling (partial derivative of  $D, E$  w.r.t. atomic displacement) are assumed to be in the order  $0.1 \text{ cm}^{-1}/\text{\AA}$  and  $0.01 \text{ cm}^{-1}/\text{\AA}^2$ , consistent with the typical values<sup>45</sup> (see supplementary for details for the parameter estimation).

Unaware of the mechanism of vibronic barrier, sometimes the experimental data were forcefully fitted by a power law with log-log scaling and unreasonable values of  $n$  might be obtained. For example, if we fit the data in Fig. 3d with logarithm scaling for both  $\tau$  and  $T$ , we have an exponent  $n = 7.7$ , as shown in Fig. 5a. When the dominant vibrational mode has lower energies, the exponent can take smaller values. For instance, in Fig. 5b, the Raman process of an vibronic barrier of  $25 \text{ cm}^{-1}$  together with the direct process leads to an exponent  $n = 2.3$  by the log-log fitting. There two cases are similar to results in Ref. 46, where big exponents  $n = 7.1, 8.5$  are deduced for Er, Yb cations, and the exponential form of a  $23 \text{ cm}^{-1}$  barrier for Ho is fitted as  $\tau \propto T^{-2.9}$ . Although this fitting procedure can yield exponents close to the standard values in some cases, this example suggests that the underlying mechanism may not be the conventional Raman process. Actually, as argued in the preceding, the conventional Raman process (Fig. 2a) can hardly become dominant because of the small Debye energies in SMM systems. Generally, it can only be an accurate accounting at temperature  $T \sim 1 \text{ K}$ .

We have investigated mechanisms that can lead to unusual Raman exponents, and fitting

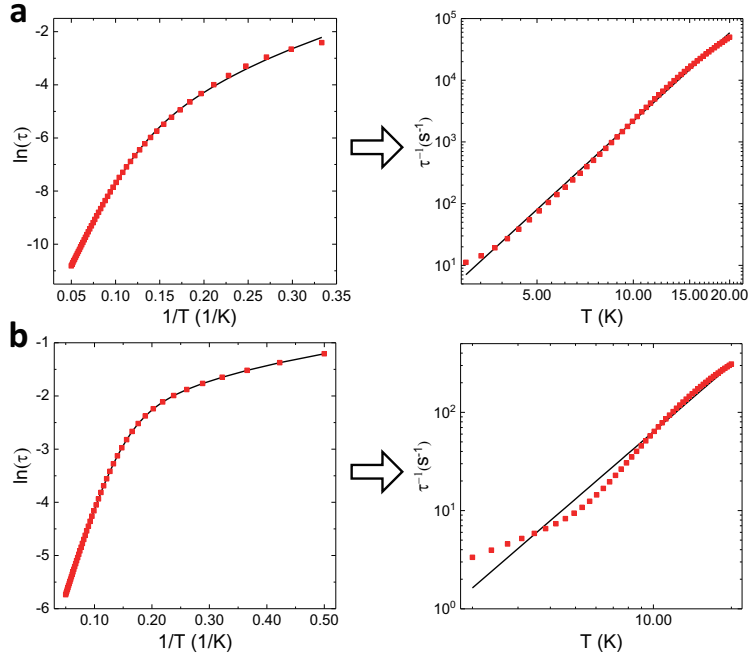


Figure 5: **a**, Fitting the data in Fig. 3d with  $\tau \propto T^{-n}$  and log-log scaling gives  $n = 7.7$ ; The closeness to the standard Raman exponents may cause misinterpretation of the underlying mechanism. **b**, For lower vibronic barriers, small exponents can be obtained; for instance, a barrier of  $25 \text{ cm}^{-1}$  leads to an exponent  $n = 2.3$ .

procedures that may mistake them. Except the high temperature exponent  $n \approx 2$ , using the power law to fit the Raman process is a misstep in general. As seen in Fig. 1c, the acoustic phonons have small DOS. Moreover, because the intra-molecule deformation is weak for acoustic phonons, the spin-phonon coupling is small. Even the high temperature exponent has limited applicability. Namely, it applies only when the lowest vibrational modes have relatively high energies, so that in a certain temperature range the high temperature expansion of  $N(\omega_q)$  is appropriate and meanwhile the vibrational modes are not thermally activated. Otherwise, the vibrational modes dominate the relaxation, and the exponential law is needed. To alleviate the effect of spin-phonon interaction, elevating energies of the vibrational modes is a designing rule, as well as using magnetic atoms with more local electronic states that are less affected by the lattice dynamics, such as some f-orbital metals.<sup>47</sup>

For the heavy lanthanide metallocenium cations<sup>46</sup> that recently receive much attention, there is an opinion that the pseudo spin Hamiltonian like  $H_S = -DS_z^2 - E(S_x^2 - S_y^2)$  is no

longer applicable due to the strong spin orbital coupling. However, as the spin operators satisfy the commute relation of angular momentum and their products form a basis (i.e., the Stevens operators<sup>48</sup>), the electronic states in these cations can still be described in the form of the pseudo spin Hamiltonian. For the irregular eigen energies that significantly deviate from the hyperbolic form ( $-DS_z^2$ ), the reason is not inapplicability of the pseudo spin formulation but large  $E$  and nonnegligible high order magnetic anisotropies. This perspective provides a clear and unified explanation to why most of the cations except the dysprosoceniums in Refs. 15,18 fail to achieve long relaxation time and molecular magnetic hysteresis. On one hand, these terms mix states  $|S_z\rangle$  ( $|S_z| \ll S$ ) into  $|\pm S\rangle$  with sizable portions to form the ground state doublet, or even result in ground state doublet no longer based on  $|\pm S\rangle$ . On the other hand, coupling between the high order magnetic anisotropies and phonons makes transitions between states with  $\Delta S_z > 2$  possible. These two factors cause a big tunneling rate between the ground state doublet, for which the magnetic hysteresis is unachievable. Noting that the calculated tunneling rates for the dysprosoceniums and the other cations do not show a clear magnitude difference,<sup>46</sup> this argument may indicate inaccuracy of the ab initio calculations for atoms with strongly localized electronic states, calling for development of numerical techniques.

In summary, because the existing theories can give rise to various Raman exponents, the subtle abnormalities have eluded researchers' attention in the study of SMMs. This leads to misuse of the power laws for fitting the  $\tau - T$  dependence in the Raman regime. The most important takeaway of this work is to abandon this misstep and deepen the understanding of the relaxation processes in different temperature regimes. As for the practical molecule design, engineering the local dynamical environment of the magnetic atom has been drawing increasing attention in recent years.<sup>1,49-52</sup> Our results demonstrate the dominant role of the vibrational modes for the magnetic relaxation in the Raman regime, which is probably most suitable for applications of SMMs. This observation highlights the cruciality of this engineerable aspect. While intricate due to complicated metal-ligand interaction, getting

rid of low energy vibrational modes and diminishing non-linear spin state-atom position dependence are general rules, as they eliminate the most effective relaxation channels and reduce the second order spin-vibration coupling, respectively.

The work is supported by the Department of Energy (grant No. DE-SC0019448) and computing time by NERSC.

## References

- (1) Escalera-Moreno, L.; Baldoví, J. J.; Gaita-Ariño, A.; Coronado, E. Spin states, vibrations and spin relaxation in molecular nanomagnets and spin qubits: a critical perspective. *Chem. Sci.* **2018**, *9*, 3265–3275.
- (2) Gaita-Ariño, A.; Luis, F.; Hill, S.; Coronado, E. Molecular spins for quantum computation. *Nature Chemistry* **2019**, *11*, 301–309.
- (3) Ardavan, A.; Rival, O.; Morton, J. J. L.; Blundell, S. J.; Tyryshkin, A. M.; Timco, G. A.; Winpenny, R. E. P. Will Spin-Relaxation Times in Molecular Magnets Permit Quantum Information Processing? *Phys. Rev. Lett.* **2007**, *98*, 057201.
- (4) Magnani, N.; Colineau, E.; Eloirdi, R.; Griveau, J.-C.; Caciuffo, R.; Cornet, S. M.; May, I.; Sharrad, C. A.; Collison, D.; Winpenny, R. E. P. Superexchange Coupling and Slow Magnetic Relaxation in a Transuranium Polymetallic Complex. *Phys. Rev. Lett.* **2010**, *104*, 197202.
- (5) Harman, W. H.; Harris, T. D.; Freedman, D. E.; Fong, H.; Chang, A.; Rinehart, J. D.; Ozarowski, A.; Sougrati, M. T.; Grandjean, F.; Long, G. J.; Long, J. R.; Chang, C. J. Slow Magnetic Relaxation in a Family of Trigonal Pyramidal Iron(II) Pyrrolide Complexes. *Journal of the American Chemical Society* **2010**, *132*, 18115–18126, PMID: 21141856.

- (6) Freedman, D. E.; Harman, W. H.; Harris, T. D.; Long, G. J.; Chang, C. J.; Long, J. R. Slow Magnetic Relaxation in a High-Spin Iron(II) Complex. *Journal of the American Chemical Society* **2010**, *132*, 1224–1225, PMID: 20055389.
- (7) Zadrozny, J. M.; Long, J. R. Slow Magnetic Relaxation at Zero Field in the Tetrahedral Complex [Co(SPh)<sub>4</sub>]<sup>2-</sup>. *Journal of the American Chemical Society* **2011**, *133*, 20732–20734, PMID: 22142241.
- (8) Lucaccini, E.; Sorace, L.; Perfetti, M.; Costes, J.-P.; Sessoli, R. Beyond the anisotropy barrier: slow relaxation of the magnetization in both easy-axis and easy-plane Ln(trensal) complexes. *Chem. Commun.* **2014**, *50*, 1648–1651.
- (9) Gómez-Coca, S.; Urtizberea, A.; Cremades, E.; Alonso, P. J.; Camón, A.; Ruiz, E.; Luis, F. Origin of slow magnetic relaxation in Kramers ions with non-uniaxial anisotropy. *Nature Communications* **2014**, *5*, 4300.
- (10) Moseley, D. H. et al. Spin–phonon couplings in transition metal complexes with slow magnetic relaxation. *Nature Communications* **2018**, *9*, 2572.
- (11) Rajnák, C.; Titiš, J.; Moncol, J.; Renz, F.; Boča, R. Slow magnetic relaxation in a high-spin pentacoordinate Fe(iii) complex. *Chem. Commun.* **2019**, *55*, 13868–13871.
- (12) Zadrozny, J. M.; Xiao, D. J.; Atanasov, M.; Long, G. J.; Grandjean, F.; Neese, F.; Long, J. R. Magnetic blocking in a linear iron(I) complex. *Nature Chemistry* **2013**, *5*, 577–581.
- (13) Blagg, R. J.; Ungur, L.; Tuna, F.; Speak, J.; Comar, P.; Collison, D.; Wernsdorfer, W.; McInnes, E. J. L.; Chibotaru, L. F.; Winpenny, R. E. P. Magnetic relaxation pathways in lanthanide single-molecule magnets. *Nature Chemistry* **2013**, *5*, 673–678.
- (14) Chen, Y.-C.; Liu, J.-L.; Ungur, L.; Liu, J.; Li, Q.-W.; Wang, L.-F.; Ni, Z.-P.; Chibotaru, L. F.; Chen, X.-M.; Tong, M.-L. Symmetry-Supported Magnetic Blocking at

- 20 K in Pentagonal Bipyramidal Dy(III) Single-Ion Magnets. *Journal of the American Chemical Society* **2016**, *138*, 2829–2837, PMID: 26883386.
- (15) Goodwin, C. A. P.; Ortu, F.; Reta, D.; Chilton, N. F.; Mills, D. P. Molecular magnetic hysteresis at 60 kelvin in dysprosocenium. *Nature* **2017**, *548*, 439–442.
- (16) Guo, F.-S.; Day, B. M.; Chen, Y.-C.; Tong, M.-L.; Mansikkamäki, A.; Layfield, R. A. Magnetic hysteresis up to 80 kelvin in a dysprosium metallocene single-molecule magnet. *Science* **2018**, *362*, 1400–1403.
- (17) Randall McClain, K.; Gould, C. A.; Chakarawet, K.; Teat, S. J.; Groshens, T. J.; Long, J. R.; Harvey, B. G. High-temperature magnetic blocking and magneto-structural correlations in a series of dysprosium(iii) metallocenium single-molecule magnets. *Chem. Sci.* **2018**, *9*, 8492–8503.
- (18) Ding, Y.-S.; Chilton, N. F.; Winpenny, R. E. P.; Zheng, Y.-Z. On Approaching the Limit of Molecular Magnetic Anisotropy: A Near-Perfect Pentagonal Bipyramidal Dysprosium(III) Single-Molecule Magnet. *Angewandte Chemie International Edition* **2016**, *55*, 16071–16074.
- (19) Bartels, L.; Meyer, G.; Rieder, K.-H. Controlled vertical manipulation of single CO molecules with the scanning tunneling microscope: A route to chemical contrast. *Applied Physics Letters* **1997**, *71*, 213–215.
- (20) Lee, H. J.; Ho, W. Single-Bond Formation and Characterization with a Scanning Tunneling Microscope. *Science* **1999**, *286*, 1719–1722.
- (21) Czap, G.; Wagner, P. J.; Xue, F.; Gu, L.; Li, J.; Yao, J.; Wu, R.; Ho, W. Probing and imaging spin interactions with a magnetic single-molecule sensor. *Science* **2019**, *364*, 670–673.

- (22) Zadrozny, J. M.; Atanasov, M.; Bryan, A. M.; Lin, C.-Y.; Rekker, B. D.; Power, P. P.; Neese, F.; Long, J. R. Slow magnetization dynamics in a series of two-coordinate iron(ii) complexes. *Chem. Sci.* **2013**, *4*, 125–138.
- (23) Ding, Y.-S.; Yu, K.-X.; Reta, D.; Ortu, F.; Winpenny, R. E. P.; Zheng, Y.-Z.; Chilton, N. F. Field- and temperature-dependent quantum tunnelling of the magnetisation in a large barrier single-molecule magnet. *Nature Communications* **2018**, *9*, 3134.
- (24) Wang, J.; Ruan, Z.-Y.; Li, Q.-W.; Chen, Y.-C.; Huang, G.-Z.; Liu, J.-L.; Reta, D.; Chilton, N. F.; Wang, Z.-X.; Tong, M.-L. Slow magnetic relaxation in a EuCu<sub>5</sub> metal-lacrown. *Dalton Trans.* **2019**, *48*, 1686–1692.
- (25) Kobayashi, F.; Ohtani, R.; Nakamura, M.; Lindoy, L. F.; Hayami, S. Slow Magnetic Relaxation Triggered by a Structural Phase Transition in Long-Chain-Alkylated Cobalt(II) Single-Ion Magnets. *Inorganic Chemistry* **2019**, *58*, 7409–7415, PMID: 31117627.
- (26) Cui, H.-H.; Lu, F.; Chen, X.-T.; Zhang, Y.-Q.; Tong, W.; Xue, Z.-L. Zero-Field Slow Magnetic Relaxation and Hysteresis Loop in Four-Coordinate CoII Single-Ion Magnets with Strong Easy-Axis Anisotropy. *Inorganic Chemistry* **2019**, *58*, 12555–12564, PMID: 31553166.
- (27) Vallejo, J.; Viciano-Chumillas, M.; Lloret, F.; Julve, M.; Castro, I.; Krzystek, J.; Ozerov, M.; Armentano, D.; De Munno, G.; Cano, J. Coligand Effects on the Field-Induced Double Slow Magnetic Relaxation in Six-Coordinate Cobalt(II) Single-Ion Magnets (SIMs) with Positive Magnetic Anisotropy. *Inorganic Chemistry* **2019**, *58*, 15726–15740, PMID: 31738531.
- (28) Abragam, A.; Bleaney, B. *Electron Paramagnetic Resonance of Transition Ions*; Oxford University Press: Oxford, 2012.

- (29) Shrivastava, K. N. Theory of Spin-Lattice Relaxation. *phys. stat. sol, (b)* **1983**, *117*, 437.
- (30) Gu, L.; Wu, R. Origins of Slow Magnetic Relaxation in Single-Molecule Magnets. *Phys. Rev. Lett.* **2020**, *125*, 117203.
- (31) Singh, A.; Shrivastava, K. N. Optical-acoustic two-phonon relaxation in spin systems. *physica status solidi (b)* **1979**, *95*, 273–277.
- (32) Blume, M.; Orbach, R. Spin-Lattice Relaxation of  $S$ -State Ions:  $Mn^{2+}$  in a Cubic Environment. *Phys. Rev.* **1962**, *127*, 1587–1592.
- (33) Chiesa, A. et al. Understanding magnetic relaxation in single-ion magnets with high blocking temperature. *Phys. Rev. B* **2020**, *101*, 174402.
- (34) Donati, F. et al. Unconventional Spin Relaxation Involving Localized Vibrational Modes in Ho Single-Atom Magnets. *Phys. Rev. Lett.* **2020**, *124*, 077204.
- (35) Vallejo, J.; Castro, I.; Ruiz-García, R.; Cano, J.; Julve, M.; Lloret, F.; De Munno, G.; Wernsdorfer, W.; Pardo, E. Field-Induced Slow Magnetic Relaxation in a Six-Coordinate Mononuclear Cobalt(II) Complex with a Positive Anisotropy. *Journal of the American Chemical Society* **2012**, *134*, 15704–15707, PMID: 22963111.
- (36) Gomez-Coca, S.; Cremades, E.; Aliaga-Alcalde, N.; Ruiz, E. Mononuclear Single-Molecule Magnets: Tailoring the Magnetic Anisotropy of First-Row Transition-Metal Complexes. *Journal of the American Chemical Society* **2013**, *135*, 7010–7018, PMID: 23586965.
- (37) Zhu, Y.-Y.; Cui, C.; Zhang, Y.-Q.; Jia, J.-H.; Guo, X.; Gao, C.; Qian, K.; Jiang, S.-D.; Wang, B.-W.; Wang, Z.-M.; Gao, S. Zero-field slow magnetic relaxation from single Co(ii) ion: a transition metal single-molecule magnet with high anisotropy barrier. *Chem. Sci.* **2013**, *4*, 1802–1806.

- (38) Fataftah, M. S.; Zadrozny, J. M.; Rogers, D. M.; Freedman, D. E. A Mononuclear Transition Metal Single-Molecule Magnet in a Nuclear Spin-Free Ligand Environment. *Inorganic Chemistry* **2014**, *53*, 10716–10721, PMID: 25198379.
- (39) Pedersen, K. S.; Dreiser, J.; Weihe, H.; Sibille, R.; Johannesen, H. V.; Sørensen, M. A.; Nielsen, B. E.; Sigrist, M.; Mutka, H.; Rols, S.; Bendix, J.; Piligkos, S. Design of Single-Molecule Magnets: Insufficiency of the Anisotropy Barrier as the Sole Criterion. *Inorganic Chemistry* **2015**, *54*, 7600–7606, PMID: 26201004.
- (40) Novikov, V. V.; Pavlov, A. A.; Nelyubina, Y. V.; Boulon, M.-E.; Varzatskii, O. A.; Voloshin, Y. Z.; Winpenny, R. E. A Trigonal Prismatic Mononuclear Cobalt(II) Complex Showing Single-Molecule Magnet Behavior. *Journal of the American Chemical Society* **2015**, *137*, 9792–9795, PMID: 26199996.
- (41) Rechkemmer, Y.; Breitgoff, F. D.; van der Meer, M.; Atanasov, M.; Hakl, M.; Orlita, M.; Neugebauer, P.; Neese, F.; Sarkar, B.; van Slageren, J. A four-coordinate cobalt(II) single-ion magnet with coercivity and a very high energy barrier. *Nature Communications* **2016**, *7*, 10467.
- (42) Krylov, D. S.; Liu, F.; Avdoshenko, S. M.; Spree, L.; Weise, B.; Waske, A.; Wolter, A. U. B.; Büchner, B.; Popov, A. A. Record-high thermal barrier of the relaxation of magnetization in the nitride clusterfullerene Dy<sub>2</sub>ScN@C<sub>80</sub>-I<sub>h</sub>. *Chem. Commun.* **2017**, *53*, 7901–7904.
- (43) Flores Gonzalez, J.; Pointillart, F.; Cador, O. Hyperfine coupling and slow magnetic relaxation in isotopically enriched DyIII mononuclear single-molecule magnets. *Inorg. Chem. Front.* **2019**, *6*, 1081–1086.
- (44) Neese, F. Software update: the ORCA program system, version 4.0. *WIREs Computational Molecular Science* **2018**, *8*, e1327.

- (45) Lunghi, A.; Totti, F.; Sessoli, R.; Sanvito, S. The role of anharmonic phonons in under-barrier spin relaxation of single molecule magnets. *Nature Communications* **2017**, *8*, 14620.
- (46) Goodwin, C. A. P.; Reta, D.; Ortu, F.; Chilton, N. F.; Mills, D. P. Synthesis and Electronic Structures of Heavy Lanthanide Metallocenium Cations. *Journal of the American Chemical Society* **2017**, *139*, 18714–18724, PMID: 29182861.
- (47) Liddle, S. T.; van Slageren, J. Improving f-element single molecule magnets. *Chem. Soc. Rev.* **2015**, *44*, 6655–6669.
- (48) Stevens, K. W. H. Matrix Elements and Operator Equivalents Connected with the Magnetic Properties of Rare Earth Ions. *Proceedings of the Physical Society. Section A* **1952**, *65*, 209–215.
- (49) Escalera-Moreno, L.; Suaud, N.; Gaita-Ariño, A.; Coronado, E. Determining Key Local Vibrations in the Relaxation of Molecular Spin Qubits and Single-Molecule Magnets. *The Journal of Physical Chemistry Letters* **2017**, *8*, 1695–1700, PMID: 28350165.
- (50) Parker, D.; Suturina, E. A.; Kuprov, I.; Chilton, N. F. How the Ligand Field in Lanthanide Coordination Complexes Determines Magnetic Susceptibility Anisotropy, Paramagnetic NMR Shift, and Relaxation Behavior. *Accounts of Chemical Research* **2020**, *53*, 1520–1534, PMID: 32667187.
- (51) Yu, K.-X.; Kragoskow, J. G.; Ding, Y.-S.; Zhai, Y.-Q.; Reta, D.; Chilton, N. F.; Zheng, Y.-Z. Enhancing Magnetic Hysteresis in Single-Molecule Magnets by Ligand Functionalization. *Chem* **2020**, *6*, 1777 – 1793.
- (52) Lunghi, A.; Sanvito, S. Multiple Spin-Phonon Relaxation Pathways in a Kramer Single-Ion Magnet. 2020.

# Support information for 'Origins of anomalous Raman exponents in single molecule magnets'

## The high temperature limit

Substituting  $|a_{qq'}| \propto \omega_q \omega_{q'}$  and the Debye phonon Density in to the main text Eq. (2), we have for the Raman process

$$p \propto N(\omega) \iint d\omega_q d\omega_{q'} k_B T \omega_q^2 \omega_{q'}^2 \omega_\Delta \delta(\omega + \omega_q - \omega_{q'}), \quad (3)$$

where  $\omega_\Delta$  is energy splitting between the ground state doublet, and  $\omega = \omega_\Delta$  specifying the transition energy. At high temperature,  $N(\omega_\Delta) \approx k_B T / \omega_\Delta$ , and the above equation gives  $\tau^{-1} = p \propto T^2$ .

## Double phonon process vs. Raman process

Assuming  $\omega_D = 10 \text{ cm}^{-1}$  and constant spin-phonon coupling strength, in the following figure we plot the transition rate between the ground state doublet of energy difference  $\omega_\Delta$ . When  $T > 3 \text{ k}$ , the intersection points are almost insensitive to  $\omega_\Delta$ , and locate at  $\omega_\Delta / \omega_D \approx 0.7$ . When  $T < 3$ , the critical ratio can be considerably lowered, indicating possible dominance of the double phonon process.

## Strengths of the relaxation channels

We take the  $S = 3/2$  for instance to show typical strength of the Orbach, Raman, and direct processes. We consider the setting of measuring the ac susceptibility, i.e., an external

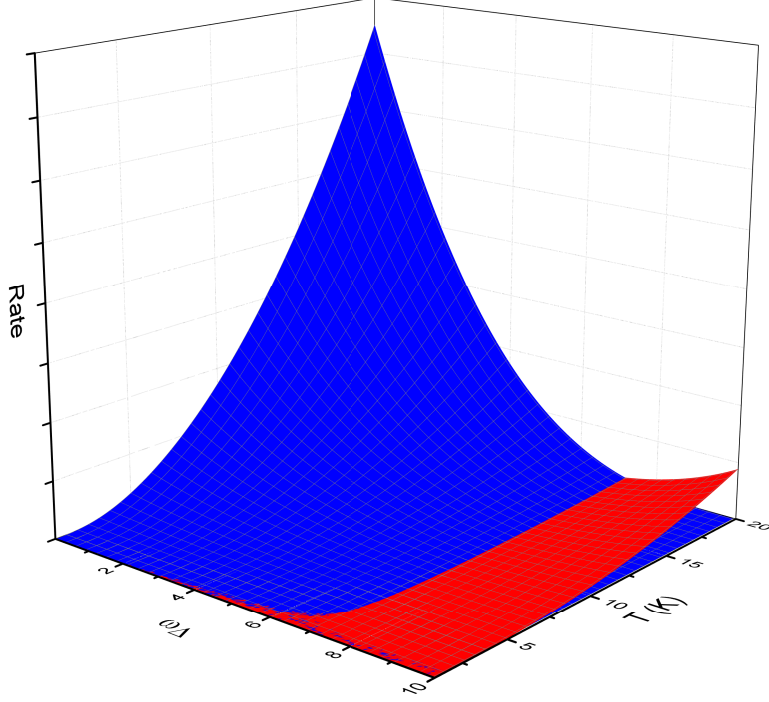


Figure 6: When  $\omega_{\Delta}/\omega_D \gtrsim 0.7$ , tunneling rate due to the double phonon process (red) can surpass the Raman process (blue). This critical ratio is reduced at low temperature.

magnetic field is performed, which is assumed to be 1000 Oe. The Hamiltonian is give by

$$H_{spin} = -DS_z^2 - E(S_x^2 - S_y^2) + \mu\mathbf{B} \cdot \mathbf{S}. \quad (4)$$

We use the parameter values in Ref. 41, that is,  $D = 115 \text{ cm}^{-1}$  and  $E = 0.01D$ . The first and second order spin-phonon coupling is given by  $C_1 = \partial H_{spin}/\partial V_q$  and  $C_2 = \partial^2 H_{spin}/\partial V_q \partial V_{q'}$ , where  $V_q$  denotes mode displacements. Eq. (4) is the standard form of **SDS**, where the **D** matrix is diagonalized by properly setting the coordinate system. As the derivative is not necessarily diagonal, we use  $\partial \mathbf{D}/\partial V_q = \lambda \mathbf{1}$  for estimation of the typical values, where **1** is the matrix with every element being 1. For the first order coupling, we set  $\lambda_1 = 0.2 \text{ cm}^{-1}/\text{\AA}$  based on the calculation in Ref. 45. As the second order coupling is hard to access, we consider a range  $\lambda_2 = 0.02 \sim 0.2 \text{ cm}^{-1}/\text{\AA}^2$ .

Taking the Orbach, Raman, and direct process together, the relaxation rate is given by

$$r = r_O e^{-U_O/k_B T} + \sum_v r_v e^{-U_v/k_B T} + r_d T, \quad (5)$$

where  $U_O$  is the Orbach barrier and  $U_v$  denotes energies of the vibrational modes. The coefficients are given by (see Ref. 30)

$$\begin{cases} r_O = \frac{2\pi|a_O|^2 \rho(U_O)}{\hbar U_O} \\ r_v = \frac{|a_v|^2}{U_v \Gamma_v} \\ r_d = \frac{2\pi k_B |a_d|^2 \rho(\omega_\Delta)}{\hbar \omega_\Delta^2} \end{cases} \quad (6)$$

where  $\Gamma_v$  denotes the square of broadening of a vibrational modes (cf. main text Fig. 1c).  $a_O$  denotes transition rate between the ground state doublet and the two excited states  $a_O = \langle g|C_1|e \rangle$  (purple arrows in main text Fig. 4a), and  $a_v$  is the transition rate within the ground state doublet due to the second order spin-phonon coupling,  $a_v = \langle g_+|C_2|g_- \rangle$ . Because of the energy conservation, only the low energy acoustic phonon can contribute to the direct process. The Orbach and the direct process both arise from the first order spin-phonon coupling. As the relative motion of atoms in an acoustic mode is much smaller than the optical modes (local vibrations), we set  $\lambda'_1 \approx 0.1\lambda_1$ , and hence  $a_d = \langle g_+|C'_1|g_- \rangle$ . Setting the broadening as  $U_v \Gamma_v = 3000 \text{ cm}^{-3}$  and use an effective atom mass of  $m = 50 \text{ amu}$  (implicitly contained in  $V_q$ ), we have

$$\begin{cases} r_O \approx 3.7 \times 10^4 \text{ ns}^{-1} \\ r_v \approx 6.2^{-2} \sim 6.2 \text{ ns}^{-1} \\ r_d = 1.8^{-2} (\text{nsK})^{-1} \end{cases} \quad (7)$$

for which we further set  $\rho(U_0) = 100\rho(\omega_\Delta)$  since a small  $\omega_\Delta$  corresponds to small  $\rho(\omega_\Delta)$  (cf. main text Fig.1c). These values give  $r_O/r_d = 6.4 \times 10^6$  and  $r_v/r_d = 3.6 \sim 360$ . In the main

text Fig.4b,  $r_O/r_d = 1.0 \times 10^7$  and  $r_v/r_d = 50$  are used, which are comparable with this general estimation and approximately reproduce the experimental data.

Because of the exponential decaying form of the second term of Eq. (5), only the lowest vibrational modes are effective. We used the frequencies calculated with the ORCA package. The def2-SVP basis set and def2/J auxiliary basis are used. The calculation is implemented at the DFT level with the PBE functional. According to the result, there are 24 modes having energies lower than the  $230 \text{ cm}^{-1}$  Orbach barrier as listed in the following Table (in  $\text{cm}^{-1}$ ).

26.6	37.9	43.9	52.6	76.2
84.9	89.7	90.3	96.7	108.7
110.2	114.4	115.5	115.7	131.8
136.1	156.1	164.0	175.1	180.3
206.7	217.4	224.5	225.4	-